Journal of Colloid and Interface Science 394 (2013) 115–123

Contents lists available at SciVerse ScienceDirect

Journal of Colloid and Interface Science

www.elsevier.com/locate/jcis

Self-assembly of resins and asphaltenes facilitates asphaltene dissolution by an organic acid

Sara M. Hashmi *, Abbas Firoozabadi *

Department of Chemical & Environmental Engineering, Yale University, New Haven, CT 06510, United States

ARTICLE INFO

Article history:
Received 23 August 2012
Accepted 28 November 2012
Available online 28 December 2012

Keywords:
Asphaltenes
Self-assembly
Colloidal stability
Non-polar electrostatics

ABSTRACT

Asphaltene precipitation occurs in petroleum fluids under certain unfavorable conditions, but can be controlled by tuning composition. Aromatic solvents in large quantities can prevent precipitation entirely and can dissolve already precipitated asphaltenes. Some polymeric surfactants can dissolve asphaltenes when added at much lower concentrations than required by aromatic solvents. Other dispersants can truncate asphaltene precipitation at the sub-micron length scale, creating stable colloidal asphaltene dispersants. One particular asphaltene dispersant, dodecylbenzene sulfonic acid (DBSA), can do both, namely: (1) stabilize asphaltene colloids and (2) dissolve asphaltenes to the molecular scale. Acid–base interactions are responsible for the efficiency of DBSA in dissolving asphaltenes compared to aromatic solvents. However, many details remain to be quantified regarding the action of DBSA on asphaltenes, including the effect of petroleum fluid composition. For instance, resins, naturally amphiphilic components of petroleum fluids, can associate with asphaltenes, but it is unknown whether they cooperate or compete with DBSA. Similarly, the presence of metals is known to hinder asphaltene dissolution by DBSA, but its effect on colloidal asphaltene stabilization has yet to be considered. We introduce the concepts of cooperativity and competition between petroleum fluid components and DBSA in stabilizing and dissolving asphaltenes. Notably, we find that resins cooperatively interact with DBSA in dissolving asphaltenes. We use UV–vis spectroscopy to investigate the interactions responsible for the phase transitions between unstable suspensions, stable suspensions, and molecular solutions of asphaltenes.

1. Introduction

Asphaltenes, the heaviest and most aromatic components of petroleum fluid, can precipitate and deposit upon the production of petroleum from the subsurface and subsequent depressurization of the fluid, often clogging wellbores and pipelines. As such many resources have been devoted not only to understanding the parameters controlling asphaltene precipitation, but also to developing methods for its inhibition and redissolution. Given the operational definition of asphaltenes as being insoluble in medium-chain alkanes but soluble in aromatic solvents, large amounts of chemicals like toluene and xylene can inhibit asphaltene precipitation. However, given the high economic and environmental cost of such treatments, chemicals effective at lower concentrations are highly desirable.

Early investigations into low-dosage asphaltene inhibitors used a selection of amphiphilic molecules with known structure in an effort to mimic resins, naturally-occuring petroleum amphiphiles [1]. Resins are precipitated from petroleum, with asphaltenes, by propane, and have approximately half the molecular weight of asphaltenes. Experimental evidence from a combination of spectroscopy techniques and elemental analysis suggests that resins contain several fused five- and six-carbon rings in addition to alkyl chains [2,3]. The fused ring structure of resins makes them similar to asphaltenes, whose fully unsaturated rings gives them the highest degree of aromaticity of any petroleum component. By contrast, resins contain a number of saturated bonds within their fused ring systems, thereby lowering their aromaticity compared to asphaltenes [3,4]. Experimental studies suggest that resins interact favorably with asphaltenes and can alter the onset of asphaltene precipitation [5–8]. At the same time, the effectiveness of resins in preventing asphaltene precipitation may depend strongly on the details of their molecular structure [3,9,10]. Theoretical studies suggest that the resin-asphaltene interactions occur through a combination of electrostatic and dispersion effects; interactions between the σ or π orbitals of the resins with the π-bonding asphaltenes have been suggested [3]. While experimental evidence for the precise molecular nature of the asphaltene-resin interaction is somewhat lacking, π–π interactions are often used to improve material properties in aromatic, polymeric opto-electronic systems [11,12]. For instance, self-assembly in aromatic hydrocarbons like functionalized hexabenzocoronene molecules allows for improved

* Corresponding authors. Fax: +1 203 432 4387.
E-mail addresses: sara.hashmi@yale.edu (S.M. Hashmi), abbas.firoozabadi@yale.edu (A. Firoozabadi).

0021-9797/$ - see front matter © 2012 Elsevier Inc. All rights reserved.
http://dx.doi.org/10.1016/j.jcis.2012.11.069

solubility and electron transport properties [13]. Non-covalent π-bonding interactions can also improve non-linear optical activities in members of the parylene family [14]. Although resins interact with asphaltenes, synthesized, or designer dispersants are more often targeted for use in enhancing asphaltene solubility.

Several types of dispersants have been used to both stabilize and dissolve precipitated asphaltenes. Various proprietary dispersants have been shown to stabilize sedimentation and limit colloidal asphaltene growth [15–17]. In some cases, the mechanism of action has been linked to the adsorption of the non-ionic dispersant to the surface of the growing asphaltene colloids, thereby limiting further growth and aggregation [18]. Several known chemical compounds can go beyond colloidal asphaltene stabilization to enable molecular dissolution of asphaltenes in medium-chain alkanes. Two classes of chemicals in particular, nonyl-phenols and benzene sulfonic acids, can dissolve asphaltenes at concentrations much lower than required by aromatic solvents like toluene [1,19–21]. Most studies use UV–vis spectroscopy to quantify molecular asphaltene concentrations in suspension supernatants, and some identify the onset point of asphaltene precipitation with the addition of heptane. In cases where nonyl-phenols and benzene sulfonic acids are used on the same asphaltene system, the benzene sulfonic acids are found to be effective at lower concentrations [1,19–22]. Furthermore, the effectiveness of the benzene sulfonic acid increases with both the length of the alkyl chain and the acidity of the headgroup [1,19,22,23].

The 12-carbon chain variety, dodecylbenzene sulfonic acid (DBSA) has been identified as the most effective of its class, showing promise for low-dosage inhibition of asphaltene precipitation [19,24]. Most previous work with DBSA has investigated its ability to dissolve asphaltenes to the molecular scale. Metal content has been identified as an important factor in determining DBSA effectiveness: removing metals increases asphaltene dissolution rates by DBSA [25,26]. Molecular modeling of DBSA has linked its dissolution effectiveness to a non-specific adsorption process that may involve layers of DBSA on the asphaltene surface [1,21,27,28]. Turbidity measurements show that low concentrations of DBSA ($\leqslant$500 ppm) do not prevent fast sedimentation of asphaltenes [15]. This result suggests the formation and aggregation of colloids, but stabilization of those colloids at intermediate DBSA concentrations is not examined. We have recently investigated the effect of DBSA in systems of asphaltenes isolated from their native petroleum fluids: in the absence of resins, colloidal asphaltene stabilization occurs at acid concentrations less than required for full asphaltene dissolution. Furthermore, UV–vis spectroscopy reveals the importance of acid–base interactions in providing both colloidal stability and molecular dissolution [29]. Now that acid–base interactions have been established experimentally, many open questions can be explored regarding the effect of mixture composition, including the effect of resins, on chemical interactions and ultimate efficacy of DBSA in stabilizing and dissolving asphaltenes.

In this work, we investigate the action of DBSA on asphaltenes precipitated by the addition of heptane to three petroleum fluids with varying physical properties, thus revealing the effect of the native petroleum resins. By measuring both dissolution and colloidal particle characteristics as a function of added DBSA, we elucidate a transition from unstable colloidal suspensions, to stable colloidal suspensions, to fully dissolved molecular solutions. Through UV–vis spectroscopy, we find intriguing suggestions regarding the importance of asphaltene composition and the cooperation and competition between resins, metals, and DBSA in interacting with asphaltenes. These molecular interactions can have profound effects on mesoscopic and macroscopic stability against asphaltene precipitation. Resins can cooperate with DBSA to facilitate low-dosage dissolution, while metals may hinder resin-asphaltene interactions. On the other hand, low resin and high metal content enables DBSA to stabilize colloidal asphaltenes before the onset of asphaltene dissolution.

2. Materials and methods

2.1. Materials

We obtain three petroleum fluids, which we call SB, QAB, and CV and measure the asphaltene and metal content, as well as their densities and the densities of the asphaltenes.

We precipitate asphaltenes by adding heptane and define the heptane ratio χ, with units mL/g, indicating the number of mL of heptane (Fischer) combined with 1 g of oil. The asphaltene content is measured as reported previously, by mixing the oil with heptane at $\chi = 40$ mL/g [16]. The mixtures are sonicated for 1 min and filtered through 0.2 μm pore-size cellulose nitrate membrane filters (Whatman). The filtrate is collected, dried, and weighed to give a fraction of asphaltenes in the oil f for each of the three petroleum fluids, as listed in Table 1: for SB $f = 0.0069$, for QAB $f = 0.0125$, and for CV $f = 0.1180$.

The density of the petroleum fluids is measured using a densitometer (Anton Paar), giving $\rho_o = 0.844$ g/mL for SB, 0.865 for QAB, and 0.905 for CV. The density ρ_a of the asphaltenes is measured by preparing a solution of 0.005 g asphaltenes per g toluene and measuring the density of the mixture. Results are based on 10–12 measurements, and the asphaltene densities are $\rho_a = 1.1 \pm 0.09$ g/mL for SB asphaltenes, 1.1 ± 0.001 for QAB, and 1.2 ± 0.08 for CV. These results are within error bars of typical values presented in the literature [30,31,17]. Table 1 includes water content results in ppm, as measured by Karl Fischer titration in Hydranal Coulomat solution (Sigma Aldrich).

We send the petroleum fluids for elemental analysis at the facilities of Lubrizol in the UK. Quantitative elemental analysis was conducted using ICP-AES (inductively Coupled Plasma-Atomic Emission Spectroscopy) following the procedure laid out in ASTM D5185 (attached). Samples were dissolved in kerosene and analyzed against a series of known standards. The content of elemental components Na, Si, P, Ca, V, Fe, Ni, and Zn is shown in Table 2 and discussed below.

Heteroatomic N and S content of isolated asphaltenes is measured by Robertson Microlit Laboratories, along with C and H content. The asphaltenes are first isolated from the petroleum fluids by mixing with heptane at $\chi = 40$ mL/g followed by filtration. C, H, and N content are measured using approximately 1 mg of sample (Cahn Electrobalance) in a CHN Analyzer (Perkin-Elmer 2400). S is measured by oxygen combustion followed by titration of barium acetate into a dimethylsulfonazo III indicator solution. The results in % are shown in Table 3.

The results of SARA analysis on all three petroleum fluids are shown in Table 4. The method follows ASTM D7419, with a few modifications, carried out by the Intertek Westport Technology Center. Heptane is used to precipitate and quantify the asphaltene fraction, followed by HPLC quantification by Evaporative Light Scattering Detection (ELSD). Our measurements of the asphaltene fractions, as shown in Table 1, are comparable to those measured by Intertek (Table 4) for CV and SB, while the value for QAB is off

Table 1
Material properties of the petroleum fluids: density ρ_o, asphaltene content f and asphaltene density ρ_a. Water content is listed in ppm.

Petroleum fluid	ρ_o (g/mL)	f (g/g)	ρ_a (g/mL)	Water (ppm)
SB	0.844	0.0069	1.1 ± 0.09	989
QAB	0.865	0.0125	1.1 ± 0.001	62
CV	0.905	0.1180	1.2 ± 0.08	2750

Table 2
Metal contents of the three petroleum fluids, as measured by ICP-AE spectroscopy. All values are listed in ppm.

Petroleum fluid	V	Fe	Ni	Zn	**Total**
SB	1	0	3	2	**6**
QAB	17	0	5	1	**23**
CV	26	4	18	365	**413**

Table 3
Elemental contents of the asphaltenes isolated from the three petroleum fluids. All values are listed in weight percent.

Asphaltene source	C	H	N	S
SB	83.89	7.90	0.16	1.49
QAB	84.43	8.47	0.67	6.82
CV	80.51	9.94	0.83	2.63

Table 4
SARA analysis of the petroleum fluids: saturates, aromatics, resins and asphaltene concentrations in weight percent.

Petroleum fluid	Saturates	Aromatics	Resins	Asphaltenes
SB	73.05	21.43	4.59	0.93
QAB	49.25	37.62	10.49	2.64
CV	48.25	27.33	13.31	11.11

by a factor of 2. This could be due to sample-to-sample variations within this particular petroleum fluid; the source field for QAB has tremendous point-to-point variations.

We obtain dodecylbenzene sulfonic acid (DBSA), with molecular weight 348 (Acros Organics). We prepare stock solutions of DBSA in heptane at various concentrations c in ppm by weight. We use dynamic light scattering (DLS) to measure the critical micelle concentration (cmc) of the DBSA in heptane.

2.2. Sample preparation

To investigate the effect of DBSA in whole asphaltene suspensions, we mix the petroleum fluids with heptane to generate asphaltenes, maintaining a constant asphaltene volume fraction $\phi \sim 0.0002$. Due to the variation of f between the three petroleum fluids, we combine them with heptane at $\chi = 30$ mL/g to make SB suspensions, 100 mL/g for QAB, and 600 mL/g for CV. Suspensions are prepared at volumes of 3 mL and sonicated for 1 min immediately before measurements are performed. We combine heptane with the stock dispersant solutions at various ratios to assess the effect of DBSA at concentrations between $10 < c < 10{,}000$ ppm.

2.3. Dynamic light scattering

We assess the effect of DBSA on colloidal asphaltene stability using phase-analysis light scattering (PALS) to measure the electrophoretic mobility μ of the asphaltene colloids (ZetaPALS, Brookhaven Instruments). PALS uses a method similar to laser doppler velocimetry to obtain μ, enabling measurements in low-dielectric media like heptane and petroleum fluids. To characterize the size a of the particles, we use dynamic light scattering (DLS) at wave vector $q = 0.01872$ nm^{-1} (ZetaPALS, Brookhaven Instruments). As done previously in the literature, we determine the DBSA concentration region appropriate for light scattering measurements, by monitoring I/I_0 in mixtures with various concentrations of DBSA [29]. The decrease in I/I_0 with an increasing amount of acid indicates the dissolution of the asphaltene colloids and subsequent darkening of the solution, which eventually becomes too dark to use light scattering methods effectively. For this reason, we can use the measurement of I/I_0 as one method to determine the transition from colloidal suspension to molecular solution, as discussed further below. Due to the colloidal instabilities in suspensions with little or no DBSA, all light scattering measurements are performed immediately after sample preparation.

We measure c_c, the critical micelle concentration, of DBSA in heptane by monitoring the normalized intensity of scattered light I/I_0 at a wave vector $q = 0.02320$ nm^{-1} (ALV Instruments). We find the cmc to be near $c_c \sim 100$ ppm for DBSA in heptane [29].

2.4. Bulk sedimentation

To assess the effect of DBSA on the bulk sedimentation of asphaltenes in heptane, we prepare whole asphaltene suspensions as noted above, with a total heptane volume of 13.8 mL. We vary c from 10 to 5000 ppm. We monitor the sedimentation front height h as a function of time on a log scale, with $t = 0$ min being the time of sample preparation. As in previous studies, sedimentation measurements are done under ambient lighting, with the aid of a cathetometer and micrometer [16,17]. All samples have an initial height $h_0 = 106$ mm.

2.5. UV–vis spectroscopy

To assess the spectroscopic qualitites of the DBSA-asphaltene suspensions, we prepare whole asphaltene suspensions as noted above, with a total heptane volume of 13.8 mL, varying c from 10 to 5000 ppm. After reaching sedimentation equilibrium at $t \sim 10^5$ min, we measure the UV–vis spectra of the suspension supernatants, in a wavelength range $190 < \lambda < 1100$ nm (Agilent 8453). The signature of DBSA alone falls at wavelengths less than 280 nm [29].

All measurements are carried out at room temperature and pressure.

3. Results and discussion

3.1. Molecular dissolution

We assess asphaltene dissolution by DBSA through inspecting the asphaltene suspensions and solutions for the presence of sediment. Rather than simply centrifuging the mixtures, we assess the sedimentation dynamics as a function of time, to investigate colloidal stability in addition to dissolution behavior. Linear sedimentation dynamics suggest stable colloids, while sedimentation fronts which suddenly collapse or fall with non-linear dynamics suggest aggregation and gelation [32,33].

Previous studies on several different combinations of asphaltenes and dispersants reveal qualitatively different sedimentation dynamics in stable as compared to unstable colloidal asphaltene suspensions. Without enough stabilizing dispersant, the sedimentation front h falls from the top of the sample, following power-law dynamics and reaching its equilibrium value within only a few hours after sample preparation [16,17]. However, with dispersant that stabilizes asphaltene colloids, any evidence of sedimentation can take much longer to appear and does so as the particles pile up at the bottom of the sample chamber. This change in sedimentation dynamics occurs with the suppression of colloidal aggregation and gelation in the suspensions [17].

We assess the effect of DBSA on the bulk sedimentation of whole asphaltenes suspensions and describe its effect on whole suspensions made with SB, as seen in Fig. 1a. As the amount of DBSA is increased up to $c = 500$ ppm, the power-law collapse of the sedimentation front persists until $t \sim 1000$ min, at which time

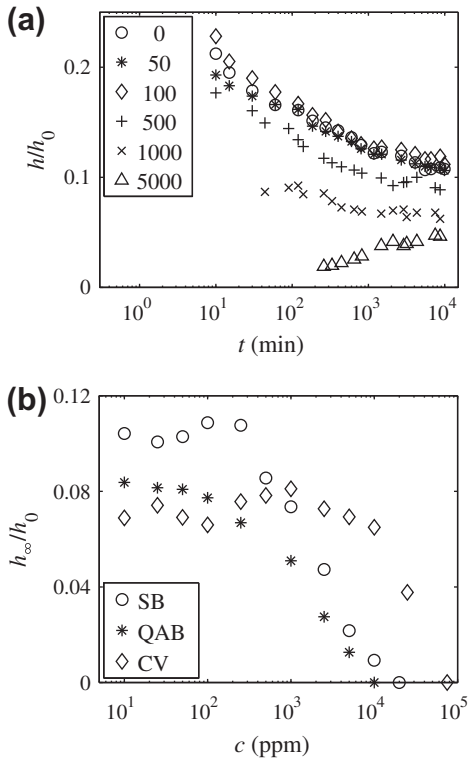

Fig. 1. Bulk sedimentation of asphaltene suspensions with DBSA: (a) shows sedimentation dynamics of SB asphaltene suspensions with DBSA at concentrations as listed in the legend; and (b) shows equilibrium sediment heights at $t \sim 6 \times 10^4$ min.

the normalized height h/h_0 begins to plateau. At c = 1000 ppm, the sedimentation front first becomes visible at approximately the same height as it remains for the duration of the measurement. At c = 5000 ppm, the sedimentation behavior qualitatively changes from a falling front to a rising front. However, while the sedimentation dynamics change from a falling to a rising front, there is no significant delay imposed on the process by the dispersant, contrary to the situation in stabilized colloidal asphaltene suspensions. QAB behaves similar to SB, while in CV, the falling sedimentation dynamics give way to a delayed rising front at as low as $c \sim 100$ ppm DBSA.

The equilibrium sedimentation behavior of whole asphaltene suspensions with DBSA gives an indication of asphaltene dissolution. As can be seen in Fig. 1a, an increase in c leads to a decrease in the equilibrium sediment amount h/h_0. We quantify this effect by measuring h_∞, the value of h at $t \sim 6 \times 10^4$ min. Given this length of time and the density difference between asphaltenes and heptane, we use the Stokes sedimentation velocity to give an order of magnitude estimate for the particle sizes in the sediment. Doing so suggests that any particles larger than ~50 nm will be incorporated in the sediment. At c < 500 ppm, h_∞ is roughly constant for each of the three types of whole asphaltene suspensions, as seen in Fig. 1b. However, beyond some threshold, the equilibrium amount of sediment decreases until no sediment is seen even at $t \sim 6 \times 10^4$ min. For whole asphaltene suspensions of SB and QAB, this threshold value is $c \sim 250$ and 100 ppm respectively, while for CV, it is nearly $c \sim 10{,}000$ ppm. At $c \sim 10{,}000$ ppm, no sediment is observed in whole suspensions of either SB or QAB after 6 weeks. For CV suspensions, c = 100,000 ppm is required to fully dissolve the asphaltenes.

Interestingly, the fast falling front seen in the SB asphaltene suspensions in Fig. 1a, even at c up to 1000 ppm DBSA, indicates that DBSA does not significantly stabilize this system. Previous investigation has revealed that the fast falling sedimentation front indicates a signature of colloidal asphaltene instability: dynamic light scattering measurements reveal colloidal aggregation in suspensions which also exhibit the fast falling sedimentation dynamics [17]. This observation has also been noted in other types of colloidal gels and suspensions [34]. The sedimentation of single, non-aggregated colloids occurs in a linear fashion, where h falls linearly with time [32].

3.2. Colloidal stability

Given the presence of sediment, and therefore, colloidal particles, at c up to 5000 ppm, we use DLS to quantify colloidal stability as a function of DBSA concentration. However, because sedimentation reveals asphaltene dissolution, we take care to avoid measuring suspensions which absorb light too strongly to give effective scattering results [29]. An assessment of the normalized scattered light intensity I/I_{max} indicates the concentration range of DBSA which forms effectively scattering colloidal suspensions. At c < 100 ppm, $I > 0.85 I_{max}$ for all three whole suspensions, indicating effective scattering off of colloidal asphaltenes. Beyond $c \sim 100$ ppm in suspensions of SB and QAB, I/I_{max} falls well below 0.8, as seen in Fig. 2. Whole CV suspensions remain effectively scattering until $c \sim 2500$ ppm.

DLS measurements on whole asphaltene suspensions reveal aggregation, as suggested by sedimentation dynamics. However, the behavior of SB and QAB asphaltene suspensions is markedly different from CV asphaltene suspensions. In SB and QAB suspension, the colloidal asphaltenes are unstable at all concentrations even approaching the onset of dissolution. For CV asphaltene suspensions, DBSA can stabilize the colloidal asphaltenes at intermediate concentrations. For example, in SB suspensions, colloidal asphaltene particle size at c = 0 ppm begins at 1.265 ± 0.378 μm, and the colloids begin to aggregate within minutes after suspension preparation. Even with c = 100 ppm, approaching the onset of asphaltene dissolution, the colloids aggregate within minutes after suspension preparation. This behavior, shown in Fig. 3a, is compatible with the non-linear sedimentation dynamics shown in Fig. 1a, which indicate aggregation. By contrast, as little as c = 25 ppm is sufficient to stall aggregation in the CV suspensions until between 15 and 20 min after sample preparation. Beyond c = 100 ppm and up to dissolution onset at c = 2500 ppm, colloidal aggregation ceases entirely. This behavior is seen in Fig. 3b and suggests slow sedimentation of CV asphaltenes, in contrast to the fast sedimentation observed in SB and QAB.

The stability of colloidal CV asphaltenes can also be seen when assessing a_0, the pre-aggregate particle size as a function of DBSA concentration. Below c = 100 ppm, $a_0 > 2$ μm for the CV asphaltenes, with large error bars. At $c \geqslant 100$ ppm, a_0 falls below 1 μm,

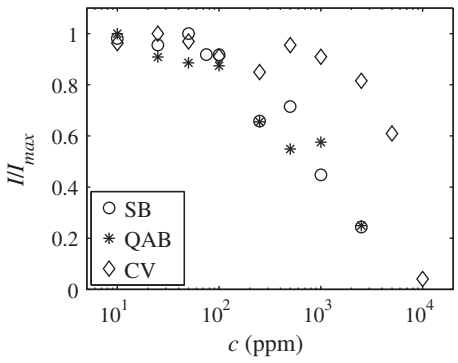

Fig. 2. Scattered light intensity of whole asphaltene suspension in heptane as a function of DBSA concentration.

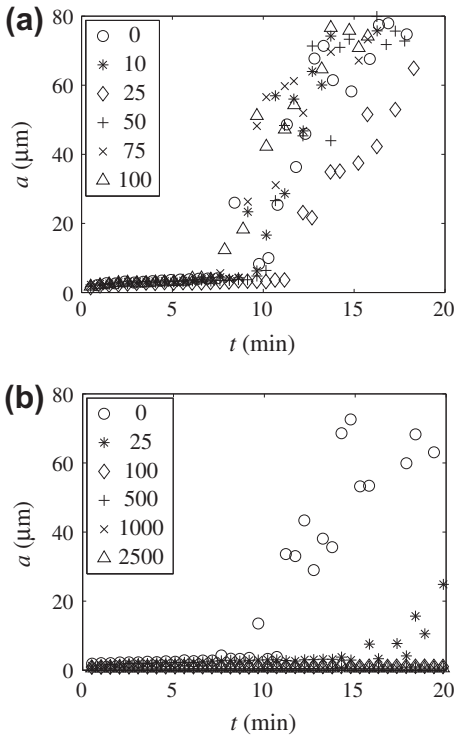

Fig. 3. Colloidal aggregation behavior of whole asphaltene suspensions with DBSA: (a) shows SB suspensions, and (b) shows CV suspensions. The legend in each indicates the DBSA concentration.

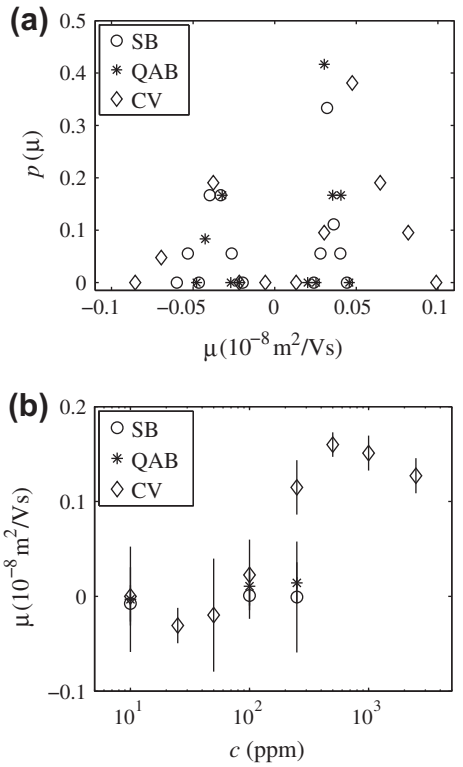

Fig. 5. Electrophoretic mobility: (a) shows a histogram of mobility measurements in each of the three whole asphaltene suspensions at c = 100 ppm and (b) shows $\langle\mu\rangle$ as a function of DBSA concentration.

and the suspensions are stable against aggregation. For CV asphaltenes, a_0 seems to plateau at 854 ± 195 nm at $c \geqslant 100$ ppm. This is not the case with colloidal asphaltenes from SB or QAB: even up until the onset of dissolution, $a_0 > 2$ μm, and aggregation occurs within approximately 10 min. This behavior alone gives a clear indication that DBSA does not provide colloidal stability to SB and QAB asphaltenes, as shown in Fig. 4. As a point of comparison, some non-ionic dispersants can effectively delay colloidal asphaltene aggregation in concentrations as low as 100 and even 10 ppm [18,35].

The colloidal asphaltene aggregation reveals the presence of attractive interparticle interactions between the colloids. We may gain insight into the rapid aggregation in whole asphaltene suspensions by measuring the electrophoretic mobility μ of the asphaltene colloids. In the absence of dispersant, the asphaltene colloids exhibit a bimodal distribution of μ, with ~50% of the measurements yielding a positive value and 50% negative [35]. The addition of DBSA does not significantly alter μ, which exhibits a bimodal distribution even at 100 ppm, close to asphaltene dissolution onset for both SB and QAB suspensions. Furthermore, the magnitude of each peak in μ is small, $\sim 0.04 \times 10^{-8}$ m^2/Vs. This result is shown in Fig. 5a.

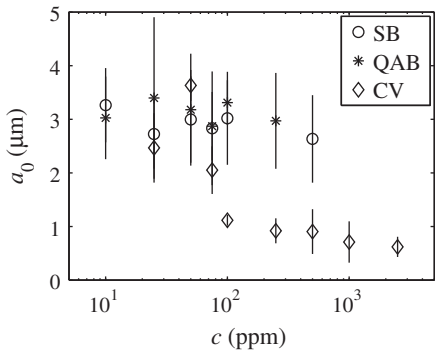

Fig. 4. Pre-aggregate colloidal asphaltene particle size as a function of DBSA concentration.

As DBSA is added to the whole asphaltene suspensions, only suspensions of type CV undergo colloidal stabilization as evidence by the aggregation measurements. This stabilization can be explained by the behavior of $\langle\mu\rangle(c)$ shown in Fig. 5b. DBSA at c = 100 ppm acts as a switch for the CV asphaltene suspensions, turning on a charging mechanism and allowing the CV colloidal asphaltenes to display a positive charge, with the plateau value of $\langle\mu\rangle \sim 0.138 \pm 0.02$ m^2/Vs above c = 100 ppm, as seen in Fig. 5b. However, no such change happens in the suspensions of SB or QAB, where $\langle\mu\rangle$ remains near 0 due to the bimodality illustrated in Fig. 5a. Interestingly, c = 100 ppm is also the critical micelle concentration of DBSA, an ionic surfactant. While the exact nature of the charging mechanism has been a matter of open debate in the literature, micelles of several other ionic dispersants are known to induce charging in colloidal particles in non-polar suspensions [36,37].

3.3. Dissolution mechanism

Several studies have suggested the importance of acid–base interactions in mediating asphaltene dissolution by DBSA and other strong organic acids [1]. We have recently confirmed the presence of acid–base interactions and quantified their importance in suspensions of isolated asphaltenes. UV–vis spectroscopy at wavelengths λ between 200–900 nm reveals the growth of a shoulder signature in the region near 400 nm, indicating the occurrence

of $n-\pi^*$ electron transitions due to acid–base interactions between the sulfonic acid and heteroatomic components in the asphaltenes [29].

In order to investigate the effect of DBSA on asphaltenes in the whole petroleum fluid, we measure the UV–vis spectra of the suspension supernatants as a function of DBSA concentration. We use the full wavelength range of our instrument in order to discern important features of the electronic spectra which could suggest the chemical mechanisms at work. As shown by our results in Fig. 6, the spectra of SB (a) and QAB (b) suspensions are markedly different from the CV (c) suspensions. Even without any DBSA, at $c = 0$ ppm, the spectra of both the SB and the QAB suspensions exhibit a shoulder in the absorbance A in the region $\lambda > 400$ nm, a feature which is lacking in asphaltene systems with neither resins nor DBSA [29]. As seen in our previous work and in studies of the doping of polyaniline with DBSA, this signature could indicate the presence of n–π^* electronic transitions at the molecular level, signifying the protonation of heteroatomic content in the asphaltenes [29,38,39]. At the same time, spectroscopic signatures in this wavelength region could also indicate π–π^* interactions, indicating stacking of ringed, aromatic molecules [40]. However, in the CV systems this signature appears only in the presence of sufficient DBSA, at concentrations above 1000 ppm. The signatures in CV are much less pronounced than those in SB and QAB. Interestingly, in isolated asphaltene suspensions, spectroscopic signatures in CV are much more prominent than in SB; this may be due to the lack of resins and therefore the lack of π–π^* transitions and also may be due to differences in heteroatom content [29].

To distinguish between the possibilities of n–π^* and π–π^* electron transitions at $c = 0$ ppm in the SB and QAB mixtures, we add a base, triethylamine (TEA). If acid–base chemistry is involved, the addition of TEA could cause additional precipitation at $c = 0$ and entirely reverse asphaltene dissolution at higher DBSA concentrations. Indeed, this effect is observed in isolated asphaltene suspensions: an equimolar addition of TEA to isolated asphaltenes dissolved in 5000 ppm DBSA causes immediate reversal of the dissolution and precipitation of the asphaltenes [29]. Similarly, the addition of TEA to whole asphaltene mixtures also reverses dissolution by DBSA and induces asphaltene precipitation in all three petroleum fluid mixtures. However, the addition of TEA to SB, QAB, and CV suspensions at $c = 0$ does not induce additional precipitation. This observation is exemplified by the addition of an excess of TEA to QAB mixtures at $c = 0$ and $c = 1000$ ppm DBSA, as shown in Fig. 7. There is no difference between the two mixtures at $c = 0$, despite the addition of TEA in the leftmost mixture. At $c = 1000$ ppm, DBSA dissolves QAB asphaltenes, as seen clearly by the color change between the two mixtures in the middle. The addition of TEA reverses this dissolution and induces asphaltene precipitation, as seen in the rightmost mixture. As in the isolated asphaltene mixtures, this observation confirms the presence of acid–base n–π^* interactions between the DBSA and asphaltenes. However, given no change with the addition of TEA at $c = 0$ ppm of DBSA, π–π^* rather than $n-\pi^*$ transitions must be responsible for the signatures at $c = 0$ in the SB and QAB mixtures. These observations confirm stacking interactions between the resins and asphaltenes in SB and QAB mixtures. Note that this π–π stacking of resins with asphaltenes neither dissolves the asphaltenes nor provides a stable suspension: the mixtures at $c = 0$ ppm DBSA are still unstable suspensions despite the π–π interactions observed in the UV–vis spectra.

In the SB suspensions at $c > 2500$ ppm, a redshift is observed in the spectral signatures, moving the shoulder out as far as 650 nm. This redshift occurs somewhat more gradually in the QAB suspensions, but also becomes dramatic at $c > 1000$ ppm. In both SB and QAB suspensions, this concentration region corresponds to significant asphaltene dissolution as observed in both the sedimentation and light scattering results (Figs. 1 and 2). Redshifts can be induced by π–π^* transitions [40]. As such, the redshift seen in SB and QAB with $c > \sim 1000$ ppm DBSA can indicate a combination of n–π^*

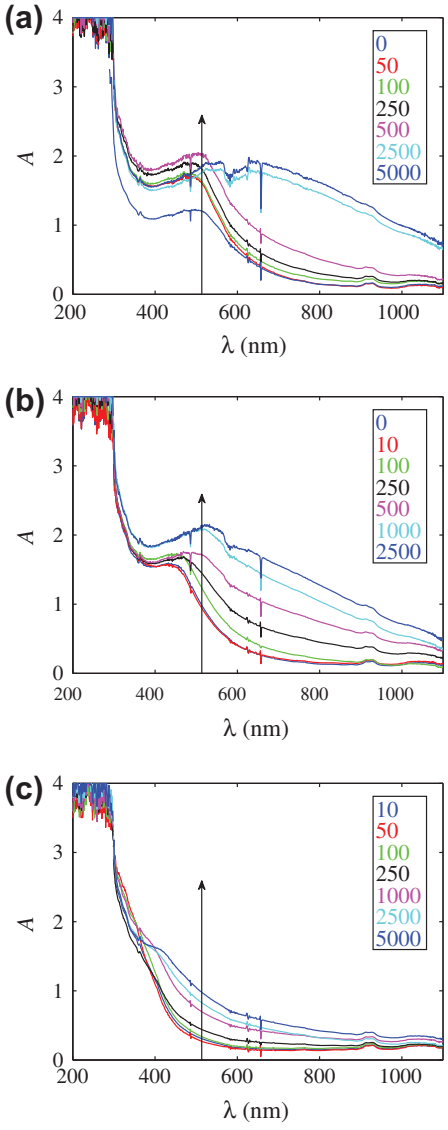

Fig. 6. UV–vis spectroscopy: (a), (b), and (c) show spectra for suspensions made with SB, QAB, and CV, respectively. In each case the legend denotes the DBSA concentration in ppm. The arrows are to guide the eye in the direction of increasing acid concentration.

Fig. 7. Addition of TEA. From left to right, the mixtures are at $c = 0$ with TEA, $c = 0$ without TEA, $c = 1000$ ppm DBSA without TEA, and $c = 1000$ ppm DBSA with TEA. All four mixtures are composed of QAB.

acid–base interactions between DBSA and asphaltenes and π–π^* stacking interactions between resins and asphaltenes. The redshift in the shoulder signature, and therefore the indication of π–π^* stacking, is absent in the CV suspensions even up to 5000 ppm.

The n–π^* acid–base interactions indicated in all three spectra denote protonation of a lone pair of electrons on a heteroatomic element (N, O, or S) contained within an asphaltene. Protonation of an asphaltene generates a positively-charged ion, which pairs with the dodecylbenzene sulfonate ion created whenever a proton leaves the strong acid DBSA. This electrostatic ion-pairing is especially strong due to the non-polar fluid background. Interestingly, despite the importance of electrostatics, water content does not seem to play a clear role in this phenomenon. Full dissolution by protonation requires more DBSA for CV than for either SB or QAB. As seen in Table 1, CV contains the most water and QAB the least. However, SB has the highest water-to-asphaltene ratio, at 0.143 g/g, while for QAB, the ratio becomes 0.005 and for CV, 0.023.

Acidity and basicity in petroleum fluids are sometimes quantified by Total Acid (TAN) and Total Base Number (TBN) measurements. Both TAN and TBN can be measured by titration of a base or an acid into a mixture of petroleum fluid, toluene, and isopropyl alcohol. TAN and TBN results are reported either as the amount or equivalent amount, respectively, of titrated potassium hydroxide solution required to facilitate color change or reach an equivalence point in a potentiometric measurement [41]. An investigation into the literature reveals that, while TAN is measured more often than TBN, the TBN in a variety of petroleum samples correlates strongly with asphaltene content, while TAN does not [41–44]. Fig. 8 shows a plot of results compiled from tables in the literature, plotted to show the dependence of TBN (a) and TBN (b) on asphaltene content f. Fig. 8a shows measurements of 29 different petroleum fluid samples, while Fig. 8b shows 20; altogether the 4 referenced papers use samples from 16 different fields worldwide. The strong correlation of TBN with asphaltene content suggests that the basic functional groups in petroleum fluids are contained largely within their asphaltene fractions. This observation lends further support to our own results that reveal the importance of asphaltenes' basic functionality for their stabilization and dissolution by an organic acid.

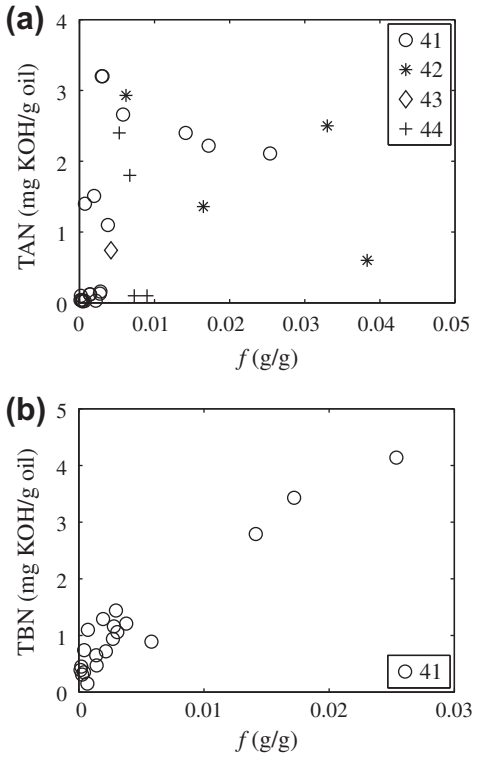

Fig. 8. TAN (a) and TBN (b) measurements as collected from literature citations, as a function of asphaltene content f (g/g) [41–44]. In each plot the corresponding sources are listed in the legend: (a) shows 29 samples from 16 different oil fields; and (b) shows 20 samples from 10 different oil fields.

3.4. Compositional effects

While SB and QAB behave similarly in terms of their colloidal asphaltene and dissolution characteristics in the presence of DBSA, CV stands out in both types of measurements, with remarkably different results. For all three petroleum fluids, asphaltene concentration and sample preparation procedures are fixed. Any differences in the results must arise from compositional differences between the three fluids themselves. A cartoon summary of the colloidal stabilization and dissolution behaviors is presented in Fig. 9. While the addition of DBSA to SB and QAB begins dissolving asphaltenes at c near 500 ppm, the phase diagram of DBSA and CV mixtures has an additional component: a stable colloidal suspension phase at $\sim 100 < c < \sim 1000$ ppm.

Being different petroleum fluids, the compositional properties of SB, QAB, and CV differ in their SARA fractions. The dissolution onset behaviors of SB and QAB are nearly identical, despite the significant differences in their saturates, resins, and asphaltenes content, as seen in Table 4. At the same time, the resin content of QAB and CV is comparable to each other, while their dissolution and phase behavior are distinctly different. However, the absolute resin content may not be as important as the weight ratio of resins to asphaltenes. In SB, this ratio is 4.9, while in QAB, the resin to asphaltene ratio is 4.0, and in CV, it is 1.2. Using literature values and assuming that resins have a molecular weight near 350, while asphaltenes have molecular weights near 750, these mass ratios become molar ratios of 12.3, 10, and 0.5 resins per asphaltene,

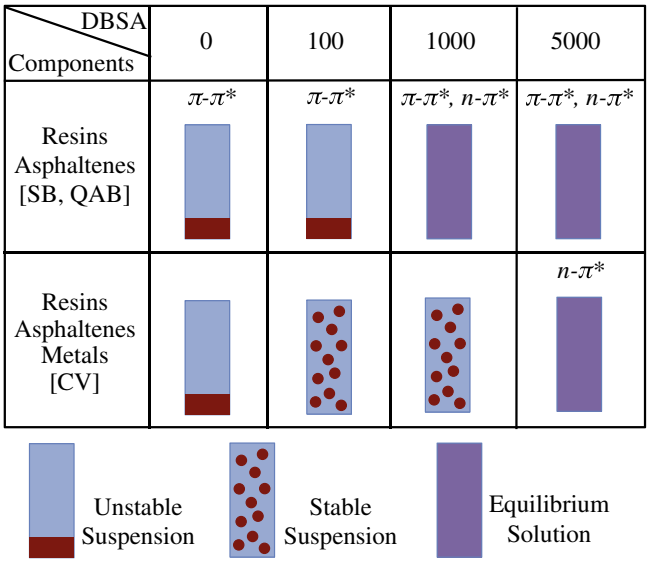

Fig. 9. Summary of compositional effects. The top row of the table gives cartoon descriptions of the action of DBSA on the asphaltenes from petroleum fluids SB and QAB, while the bottom row describes CV. The cartoon mixtures indicate the transition from unstable suspensions (in blue and red) to equilibrium molecular solutions (in purple). For CV there is an intermediate step: stable suspensions. The concentrations in ppm listed above the table are meant as order of magnitude guides to the observed behavior. (For interpretation of the references to color in this figure legend, the reader is referred to the web version of this article.)

for SB, QAB, abd CV, respectively [3,4]. The differences in resin to asphaltene ratio may help to explain the differences in the resin-asphaltene π–π^* associations seen in the UV–vis spectra. SB, with the highest amount of resins per asphaltene, has the most pronounced π–π^* shoulder at $c = 0$, while CV has nearly no signatures indicating π–π^* interactions. Furthermore, the most dramatic redshift is also seen in SB mixtures, which have the highest resin to asphaltene ratio. We can understand these differences given that the magnitude of the π–π^* signature depends on the number of interactions between resins and asphaltenes. While π–π stacking may also occur between resins and asphaltenes in CV, a molar ratio of 0.5 may not provide enough resin molecules to interact with each asphaltene, causing the electron transition signatures to be undetectable above the background.

Investigation into the resin to asphaltene ratio may also help to explain the appearance of the stable colloidal phase in CV. In isolated asphaltene systems of all three of these petroleum fluids, without any resins, DBSA first enables a stable colloidal phase before initializing dissolution [29]. The colloidal stability behavior of CV with DBSA is similar in the two cases: with and without the naturally occurring resins. Furthermore, SB and QAB asphaltenes in the absence of resins begin dissolving closer to $c \sim 1000$ ppm DBSA rather than the 100 ppm transition observed here [29]. The observations suggest that resin cooperation and self-assembly with DBSA allows asphaltene mixtures to transition directly from unstable suspensions to molecular solutions. As evidenced by the shoulders and redshift in the spectra of SB and QAB asphaltenes, the protonation of the growing π conjugated system allows for low-dosage dissolution of asphaltenes by DBSA.

Previous studies have shown that metal content affects the dissolution properties of asphaltenes: increased metal content requires larger concentrations of DBSA to effectively dissolve asphaltenes [25,26]. As highlighted in Table 2, the total metal content of CV is an order of magnitude larger than that of QAB, and two orders larger than that of SB. With this additional metal content, nearly 5000 ppm DBSA is required to dissolve CV asphaltenes, compared to 100 ppm required for SB and QAB. Even in the absence of resins, isolated asphaltenes of CV still require $\sim$3 times higher DBSA concentrations to initiate dissolution than in the case of SB and QAB [29]. The molecular mechanism may involve the asphaltene conformation induced by metallic components. The metallic content in asphaltenes, including vanadium, nickel, iron, and zinc, is found mainly in porphyrin complexes, which give an added dimensionality to the otherwise flat polyaromatic hydrocarbon rings [45,46]. Porphyrins have a steric bulk that has been observed to alter adjacent bonding parameters and even hinder oxidation processes [47,48]. While their presence would not prevent an acidic proton of DBSA from attacking asphaltenic heteroatoms, porphyrins may hinder the resultant ion-pairing of the larger DBSA anion with the cationic protonated asphaltene. Given that resins form π–π stacks with asphaltenes, and porphyrins would also sterically hinder this interaction by their three-dimensional presence on the platelike asphaltene. Even though the resin to asphaltene ratio in CV is low, the presence of metals may further hinder the ability of both resins and DBSA to interact with the asphaltenes.

Elemental analysis of the heteroatomic content in the asphaltenes of each petroleum fluid may give further insight (Table 3). The N content in the asphaltenes from the three petroleum fluids is least in the asphaltenes from SB, which require the least DBSA to dissolve, and highest in the asphaltenes from CV, which require the most DBSA for full asphaltene dissolution. The S content, however, does not strongly correlate with the amount of acid required to dissolve the asphaltenes. The stronger correlation between N and the acid requirement for full dissolution follows from the fact that N is a more basic element than S [49].

4. Conclusions

A variety of experimental methodologies reveals a transition from unstable colloidal asphaltene suspensions to completely dissolved molecular solutions upon the addition of the strong organic acid DBSA to heptane mixtures with three distinct petroleum fluids. Despite the wide range of asphaltene content spanned by the three fluids under consideration, UV–vis spectroscopy confirms the importance of acid–base interactions in facilitating this transition. Furthermore, the UV–vis results suggest that resins may cooperatively self-assemble with DBSA in forming complexes with asphaltenes to allow for low-dosage dissolution. Dynamic light scattering and bulk sedimentation measurements reveal significant differences between the three fluids, two of which transition directly from unstable suspensions to molecular solutions, while the third demonstrates a stable colloidal suspension phase at intermediate acid concentrations. Investigations into several different compositional considerations reveal the importance of the resin to asphaltene ratio and metal content in determining the presence of the stable colloidal phase. Heteroatomic nitrogen in the asphaltenes plays an important role in the acid–base interactions facilitating dissolution.

While it is commonly understood that asphaltenes have a complicated chemical composition, our current study suggests specific directions for future work in determining the efficacy of acidic dispersants for dissolving asphaltenes. Surprisingly, the effect of water may not be so important in predicting the dissolution behavior of asphaltenes as resin, heteroatomic, and metal content. Future studies using a continuum of metal and resin content could potentially quantify the cooperation between DBSA and resins, as well as the dependence of DBSA efficacy on metal content. Metal content can for instance be varied through a series of chelations and progressive filtrations [25]. Even beyond the realm of asphaltene dispersant studies, the UV–vis confirmation of π–π stacking between resins and asphaltenes may begin to clarify the nature of the oft-speculated interactions between these two highest molecular weight components of petroleum. The cooperation between π–π and acid–base interactions may apply beyond the study of asphaltenes entirely, suggesting improved mechanisms for the dissolution of conducting polymers.

Acknowledgments

We gratefully acknowledge the support of RERI member institutions, and experimental assistance from Kathy Xinyi Zhong, Salvatore DeLucia, and Anjali Khetan. SMH thanks Ulrich Hintermair for helpful conversations. We appreciate the use of the ALV light scattering equipment belonging to Menachem Elimelech, and the use of the Karl Fischer titrator in the lab of Nilay Hazari. The authors acknowledge Lubrizol for carrying out the metal content analysis and Intertek Westport Technology Center for the SARA analysis.

References

[1] C.-L. Chang, H.S. Fogler, Langmuir 10 (1994) 1749–1757.
[2] D.J. Porter, P.M. Mayer, M. Fingas, Energy Fuel 18 (2004) 987–994.
[3] O. Castellano, R. Gimon, C. Canelon, Y. Aray, H. Soscun, Energy Fuel 26 (2012) 2711–2720.
[4] O.C. Mullins, Energy Fuel 24 (2010) 2179–2207.
[5] N.F. Carnahan, Energy Fuel 13 (1999) 309–314.
[6] J. Dufour, J.A. Calles, J. Marugan, R. Gimenez-Aguirre, J.L. Pena, D. Merino-Garcia, Energy Fuel 24 (2010) 2281–2286.
[7] L. Goual, A. Firoozabadi, AIChE J. 50 (2004) 470.
[8] M. Sedghi, L. Goual, Energy Fuel 24 (2010) 2275–2280.
[9] O. Leon, E. Contreras, E. Rogel, G. Dambakli, S. Acevedo, L. Carbognani, J. Espidel, Langmuir 18 (2002) 5106–5112.
[10] E. Rogel, Energy Fuel 22 (2008) 3922–3929.

[11] J.H. Olivier, J. Barber, E. Bahaidarah, A. Harriman, R. Ziessel, J. Am. Chem. Soc. 134 (2012) 6100.
[12] G. Salassa, M.J.J. Coenen, S.J. Wezengberg, B.L.M. Hendriksen, S. Speller, J.A.A.W. Elemans, A.W. Kleij, J. Am. Chem. Soc. 134 (2012) 7186.
[13] S. Ito, M. Wehmeier, J.D. Brand, C. Kubel, R. Epsch, J.P. Rabe, K. Mullen, Chem. – Eur. J. 6 (2000) 4327–4342.
[14] W. Wu, Q. Huang, G. Qiu, C. Ye, J. Chin, Z. Li, J. Mater. Chem. 22 (2012) 18486–18495.
[15] K. Kraiwattanawong, H.S. Fogler, S.G. Gharfeh, P. Singh, W.H. Thomason, S. Chavadej, Energy Fuel 23 (2009) 1575–1582.
[16] S.M. Hashmi, L.A. Quintiliano, A. Firoozabadi, Langmuir 26 (2010) 8021.
[17] S.M. Hashmi, A. Firoozabadi, J. Phys. Chem. B 114 (2010) 15780–15788.
[18] S.M. Hashmi, A. Firoozabadi, Soft Matter 7 (2011) 8384.
[19] Y.-F. Hu, T.-M. Guo, Langmuir 21 (2005) 8168–8174.
[20] G. Gonzalez, A. Middea, Colloid Surf. 52 (1991) 207–217.
[21] O. Leon, E. Rogel, A. Urbina, A. Andujar, A. Lucas, Langmuir 15 (1999) 7653–7657.
[22] T.A. Al-Sahhaf, M.A. Fahim, A.S. Elkilani, Fluid Phase Equilib. 194–197 (2002) 1045–1057.
[23] J.-A. Ostlund, M. Nyden, H.S. Fogler, K. Holmberg, Colloid Surf. A 234 (2004) 95–102.
[24] H.H. Ibrahim, R.O. Idem, Energy Fuel 18 (2004) 734–754.
[25] T.J. Kaminski, H.S. Fogler, N. Wolf, P. Wattana, A. Mairal, Energy Fuel 14 (2000) 25–30.
[26] H.H. Ibrahim, R.O. Idem, Energy Fuel 18 (2004) 1038–1048.
[27] O. Leon, E. Rogel, J. Espidel, G. Torres, Energy Fuel 14 (2000) 6.
[28] E. Rogel, O. Leon, Energy Fuel 15 (2001) 1077–1086.
[29] S.M. Hashmi, K.X. Zhong, A. Firoozabadi, Soft Matter 8 (2012) 8778–8785.
[30] T.F. Yen, G. Erdman, W.E. Hanson, J. Chem. Eng. Data 6 (1961) 443.
[31] M.S. Diallo, T. Cagin, J.L. Faulon, W.A. Goddard III, in: T.F. Yen, G.V. Chilingarian (Eds.), Asphaltenes and Asphalts, 2, vol. 40, Elsevier Science, New York, 2000, pp. 103–127.
[32] G.K. Batchelor, J. Fluid Mech. 52 (1972) 245–268.
[33] L. Starrs, W.C.K. Poon, D.J. Hibberd, M.M. Robins, J. Phys. – Condens. Matter 14 (2002) 2485–2505.
[34] S. Manley, J.M. Skotheim, L. Mahadevan, D.A. Weitz, Phys. Rev. Lett. 94 (2005) 218302.
[35] S.M. Hashmi, A. Firoozabadi, Soft Matter 8 (2012) 1878–1883.
[36] G.S. Roberts, R. Sanchez, R. Kemp, T. Wood, P. Bartlett, Langmuir 24 (2008) 6530.
[37] M.F. Hsu, E.R. Dufresne, D.A. Weitz, Langmuir 21 (2005) 4881–4887.
[38] O. Ngamna, A. Morrin, A.J. Killard, S.E. Moulton, M.R. Smyth, G.G. Wallace, Langmuir 23 (2007) 8569–8574.
[39] S.E. Moulton, P.C. Innis, L.A.P. Kane-Maguire, O. Ngamna, G.G. Wallace, Curr. Appl. Phys. 4 (2004) 402–406.
[40] X. Huang, K. Nakanishi, N. Berova, Chirality 12 (2000) 237–255.
[41] T. Barth, S. Hoiland, P. Fotland, K.M. Askvik, R. Myklebust, K. Erstad, Energy Fuel 19 (2005) 1624–1630.
[42] D. Dudasova, S. Simon, P.V. Hemmingsen, J. Sjoblom, Colloid Surf. A 317 (2008) 1–9.
[43] M. El Gamal, A.O. Mohamed, A.Y. Zekri, J. Pet. Sci. Eng. 46 (2005) 209–224.
[44] P. Juyal, V.N. Le, A.T. Yen, S.J. Allenson, J. Dispersion Sci. Technol. 32 (2011) 1096–1104.
[45] G.B. Vaughan, E.C. Tynan, T.F. Yen, Chem. Geol. 6 (1970) 203–219.
[46] P.J. Brothers, Adv. Organomet. Chem. 64 (2000) 223–321.
[47] J.P. Collman, J.I. Brauman, K.M. Doxsee, Proc. Natl. Acad. Sci. USA 76 (1979) 6035–6039.
[48] K.-L. Lay, J.W. Buchler, J.E. Kenny, W.R. Scheidt, Inorg. Chim. Acta 123 (1986) 91–97.
[49] M.B. Smith, J. March, March's Advanced Organic Chemistry, John Wiley & Sons, New Jersey, 2007, pp. 490–495.